ResearchGate

See discussions, stats, and author profiles for this publication at: https://www.researchgate.net/publication/326009870

Interpretation of free fall penetrometer tests in sands: An approach to determining the equivalent static resistance

Conference Paper · June 2018

CITATIONS
3

READS
524

3 authors:

David J White
University of Southampton
282 PUBLICATIONS **6,138** CITATIONS
SEE PROFILE

Conleth O'Loughlin
University of Western Australia
128 PUBLICATIONS **1,252** CITATIONS
SEE PROFILE

Shiao Huey Chow
University of Melbourne
36 PUBLICATIONS **261** CITATIONS
SEE PROFILE

Some of the authors of this publication are also working on these related projects:

Suction bucket foundations for offshore wind energy installations in layered soils View project

Instrumented Free Fall Sphere View project

All content following this page was uploaded by Shiao Huey Chow on 27 June 2018.

The user has requested enhancement of the downloaded file.

Cone Penetration Testing 2018 – Hicks, Pisanò & Peuchen (Eds)
© 2018 Delft University of Technology, The Netherlands, ISBN 978-1-138-58449-5

Free fall penetrometer tests in sand: Determining the equivalent static resistance

D.J. White
University of Southampton, UK

C.D. O'Loughlin
University of Western Australia, Australia

N. Stark
Virginia Tech, USA

S.H. Chow
University of Western Australia, Australia

ABSTRACT: Free Fall Penetrometer (FFP) tests provide an efficient way to determine the penetration resistance at shallow depths in sandy soils, and are being used increasingly in geotechnical, geomorphological and coastal engineering applications. A limitation of free fall penetrometers is the effect of their high velocity on the penetration resistance. This affects the drainage condition, creates a viscous-type enhancement of the mobilised strength, and also introduces inertial drag forces. It is useful if the measured FFP resistance can be adjusted back to the resistance that would be expected in a standard Cone Penetrometer Test (CPT) at the same location. With this adjustment, the resistance can be used in the same correlations and design methods as standard CPT data. Adjustments for viscous-type rate effects and inertial drag have been proposed and explored in detail for clay soils. The contribution of this paper is to outline a correction scheme for drainage condition, which is more relevant for sandy soils. This correction utilizes the dissipation response at the end of the FFP test, in combination with the measured or derived FFP tip resistance. Relationships for penetration resistance in drained and undrained conditions based on density state are developed. It is shown that the high velocity FFP resistance can be uniquely mapped to a resistance from a standard CPT, when combined with the dissipation response. With development and validation, this new framework could enhance the value of FFPs as a complementary or alternative technology alongside conventional static penetration testing.

1 INTRODUCTION

1.1 *Free fall penetrometry*

Free-fall penetrometers (FFPs) are devices that are dropped from above the seafloor and self-penetrate into the seabed. Data gathered during the deceleration, such as tip and shaft resistance, are interpreted to determine the seabed properties.

Conventional push-in penetrometers are commonly deployed using a seabed reaction frame lowered from a survey vessel. FFPs can be deployed from smaller and less expensive vessels. Also, because they allow coverage of a large seabed area in a relatively short time frame, they have particular potential in supplementing data from push-in penetrometer tests that are undertaken at large spatial intervals, reducing the uncertainty associated with spatial variability.

Most free-fall penetrometers have geometries that resemble their 'push-in' counterparts. However, the velocity at impact with the seabed is typically up to 10 m/s depending on geometry and drop height. which is almost three orders of magnitude higher than push-in penetrometers, inserted at a standard rate of 0.02 m/s.

1.2 *Interpretation in clay soils*

In soft clay seabeds, FFPs travel at undrained rates of penetration. The measured data must be interpreted in a framework that accounts for the effect of strain rate on the mobilized soil strength, within the undrained range, to determine a soil strength that is equivalent to a constant (and much lower) velocity push-in test.

Recent studies have established frameworks for making this type of correction, which include

allowance for the apparent different effects of strain rate on shaft friction and tip bearing (Steiner et al. 2014; Chow et al. 2014, Chow et al. 2017).

It has also been demonstrated that these devices can measure the coefficient of consolidation if the penetrometer remains in the seabed after installation to record the dissipation of excess pore pressure (Mulukutla 2009, Chow et al. 2014). As a result, there is now a complete framework for interpretation of an FFP in soft clay to determine the same strength and consolidation parameters as a conventional piezocone test.

1.3 *Interpretation in sandy soils*

FFPs have also been tested in sandy soils, and have proven capable of identifying subtle stratigraphic layering within the upper tens of centimetres of the seabed (Stark et al. 2009), providing a powerful tool for wide area surveys of shallow seabed geomorphology. However, to date there is no equivalent interpretation method for sands to determine a soil strength parameter from the FFP tip resistance. Instead, the tip resistance is sometimes altered for strain rate effects to determine a corrected quasi-static penetration resistance, using the same type of approach as for tests in clay.

To establish a rigorous interpretation of FFPs in sandy soils, it is necessary to introduce an additional element to the interpretation process, to allow for drainage conditions. In clay soils, both FFP tests and conventional push-in CPTs involve undrained penetration, so allowance need only be made for viscous-type strain rate effects in estimating the appropriate undrained shear strength. In contrast, FFP tests in sand generally involve undrained penetration, whereas push-in tests are generally fully drained.

To illustrate this point, the boundaries for undrained and drained penetration are shown in Figure 1 using the dimensionless velocity, $V = vD/c_h$, where v is the penetrometer velocity, D is the diameter of the penetrating object and c_h is the consolidation coefficient. For $V < 0.1$, drained conditions apply but for $V > 30$ undrained conditions apply, based on both theoretical and numerical modelling (e.g. Colreavy et al. 2015, Chatterjee et al. 2013). These criteria lead to combinations of soil type – defined by c_h – and penetrometer velocity that fall in each drainage regime.

The domain of FFP tests is illustrated as $v > 0.1$ m/s, with a reasonable upper limit being of the order of 10 m/s, whereas conventional tests adopt a standard velocity of 0.02 m/s. For sandy soils, the consolidation coefficient may lie in the range 10^4–10^6 m^2/year, which leads to undrained or partially-drained conditions during FFP penetration.

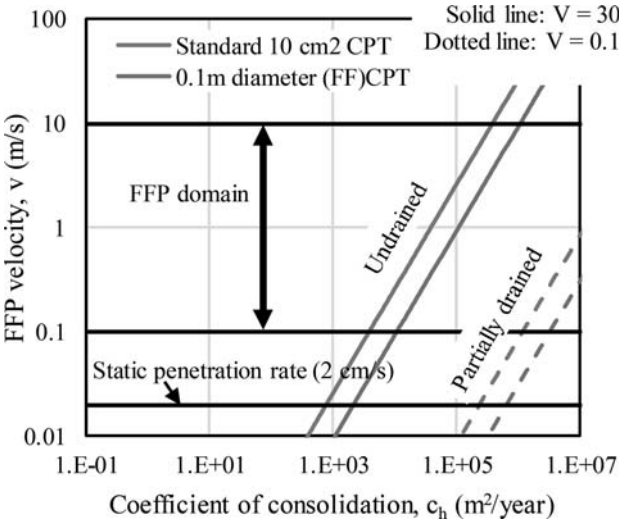

Figure 1. Drainage during penetrometer tests.

A conventional static push-in test is fully drained in sandy conditions. The u_2 pore pressure measurement provides an indication of the drainage regime, and the Robertson (1990) classification charts indicate that in sands and silty sands the normalized u_2 pore pressure ($B_q = (u_2-u_0)/q_{net}$) will not exceed ~0.2.

An FFP penetrating at a velocity that is two orders of magnitude higher, will show the pore pressure response equivalent to a much lower permeability soil, with a more significant value of B_q, that could be positive or negative, depending on whether the soils is dilatant or contractile.

1.4 *Interpretation for drainage in sandy FFP tests*

This paper outlines a new approach to allow for the effect of drainage in the interpretation of FFPs. It operates on the following basis:

1. A generic model is established for penetration resistance of the same soil in both drained and undrained conditions.
2. The model is tied to two soil parameters: relative density, I_d, and consolidation coefficient, c_h.
3. Relative density controls the penetration resistance in both drained and undrained conditions, and therefore also sets the ratio between drained and undrained resistance.
4. Consolidation coefficient controls the velocity thresholds between fully undrained, partially-drained and fully drained penetration.

Since the model has two soil parameters, they can only be uniquely defined from two FFP test measurements, and so the interpretation relies on both the dynamic penetration resistance, q_{dyn}, and also a dissipation stage immediately after the FFP comes to rest from which c_h can be determined. The

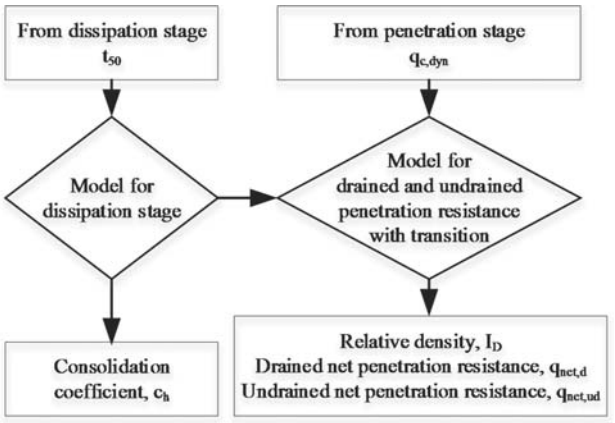

Figure 2. Interpretation scheme to allow for drainage condition.

model scheme is outlined in Figure 2. The following sections describe each element of the model.

The model is applied via example scenarios of soil that has uniform relative density with depth.

2 COEFFICIENT OF CONSOLIDATION

For a free fall cone penetrometer, the dissipation of excess pore pressure around the tip can be approximated by the following approximation to the time for 50% of the excess pore pressure to dissipate, t_{50}:

$$T_{50} = \frac{c_h t_{50}}{D^2} \rightarrow c_h = \frac{D^2 T_{50}}{t_{50}} \quad (1)$$

where T_{50} can be taken as 0.6, which is appropriate for typical values of rigidity ratio based on numerical analysis, and assumes that the prior penetration is fully undrained (Mahmoodzadeh et al. 2015).

The value of c_h determined from the dissipation data can be used to convert the velocity profile of the FFP deceleration into a profile of dimensionless velocity, V (assuming that the consolidation coefficient derived for the end of the drop also applies throughout the profile). As for static penetration tests, this idealized dissipation response can be applied to the dissipation seen in dilatant soil where an initial rise in pore pressure is often observed (Sully et al. 1999).

The penetration resistance between the undrained and drained regions can be defined using a 'backbone' curve of the form:

$$q_{net,dyn} = q_{net,ud} + \left(q_{net,d} - q_{net,ud}\right)\left(\frac{1}{1+\left(\frac{V}{V_{50}}\right)}\right) \quad (2)$$

where $V_{50} \sim 1$ (Randolph & Hope 2004).

Field studies show FFPs can provide consistent pore pressure data, despite the high velocity impact (Albatal et al. 2017), with a Bernoulli-type correction at the u_2 positon during free fall (Mumtaz et al. 2018).

3 DRAINED RESISTANCE

The drained penetration resistance, $q_{c,d}$, can be linked to the relative density via conventional correlations derived for clean sands, which are widely used in engineering practice for all sands. Many such correlations are available, which vary in their detail. The approach by Jamiolkowski et al. (2003) is adopted here:

$$I_D = \frac{1}{C_2}\ln\left(\frac{q_{net,d}}{C_0 p_0'^{C_1}}\right) \quad (3)$$

where $q_{c,d}$ and p'_0 are in kPa, and the coefficients are $C_0 = 300$ (dimensional), $C_1 = 0.46$, $C_2 = 2.96$. In our analysis, we have assumed for illustrative purposes an earth pressure coefficient of 0.5 and an in situ effective unit weight of 8 kN/m^3, meaning that $p'_0 = 5.3z$ where z is the depth below the seabed in metres.

If information on the soil mineralogy is available, the more sophisticated correlations of Mayne (2014) could be used, and other alternatives to Equation 3 exist, particularly at lower stress level and low embedment depth (e.g. Emerson et al. 2008), and may be preferred.

4 UNDRAINED RESISTANCE

The undrained penetration resistance, $q_{c,ud}$, is linked to relative density via Bolton's correlations, which provide a connection between density and angles of friction and dilation, varying with effective stress level (Bolton 1986). These correlations can be applied to determine the undrained strength of sands, by recognizing that in undrained failure the dilation angle must be zero. In Bolton's terminology, this requires a relative dilatancy, I_R, of zero, so that:

$$I_R = I_D(Q - \ln p') - 1$$
$$\text{Undrained failure}: I_R = 0 \text{ so } p'_f = e^{Q - \frac{1}{I_D}} \quad (4)$$

In silica sands, Q, referred to as the crushing strength parameter, is commonly taken as 10 (where p′ is defined in kPa) (Randolph et al. 2004). If mineralogical information is available, the value

of Q could be refined. Using the mean stress at failure, p'_f, the undrained strength can be calculated as:

$$s_u = \frac{1}{2} p'_f \left(\frac{6\sin\phi_{cv}}{3-\sin\phi_{cv}} \right) \quad (5)$$

adopting here the compressive failure criterion, and using the constant volume or critical state friction angle, ϕ_{cv}. Bolton (1986) shows this is relatively invariant for siliceous soils (31–33° with 32° adopted in this paper). For other mineralogies, alternative values are recommended (e.g. Randolph et al. 2004).

The undrained strength could also be augmented by a viscous adjustment for strain rate, following Randolph (2004) and Chow et al. (2017). Also, a cavitation criterion, dependent on the back pressure (i.e. water depth) could be used to set an upper limit on p'_f. For simplicity these additional elements have not been included in the model in the present paper.

The undrained strength can be converted to undrained penetration resistance, $q_{c,ud}$ via a conventional bearing factor, N_{kt}. We have adopted a value of $N_{kt} = 12$ which is the mean value from studies of clay soils reported by Lunne et al. (2011). However, this value is subject to the same uncertainties as for static CPTs, particularly at shallow embedment where a lower value of N_{kt} could be utilized instead (e.g. Aubeny & Shi 2006).

$$q_{net,u} = N_{kt} s_u \quad (6)$$

5 COMBINED MODEL

The analysis steps described above lead to backbone curves shown in Figure 3, which correspond to a depth of z = 2 m and use the parameters given previously.

It is notable that the backbone curves show divergent shapes at low and high relative density: in loose materials the undrained resistance is less than the drained resistance, whereas in dense materials the opposite is true. This is consistent with the effect of dilatancy, with the dense material dilating, causing a rise in effective stress and an increase in penetration resistance in undrained conditions.

The backbone curves do not cross, meaning that for any combination of q_c and V, there is a unique density state, which in turn has a pair of unique drained and undrained penetration resistances.

The transition between fully drained and fully undrained takes place over two orders of magnitude of V. Typical uncertainty in consolidation coefficient could be a factor of five, which gives

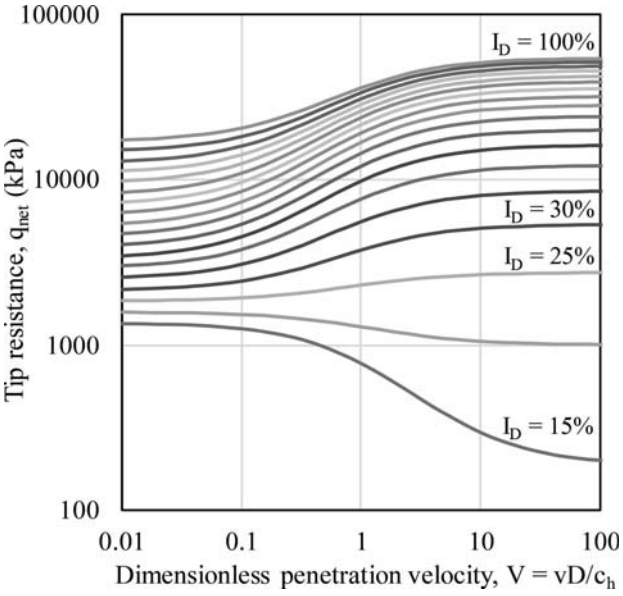

Figure 3. Example backbone curves linking dynamic penetration resistance to relative density and penetration speed.

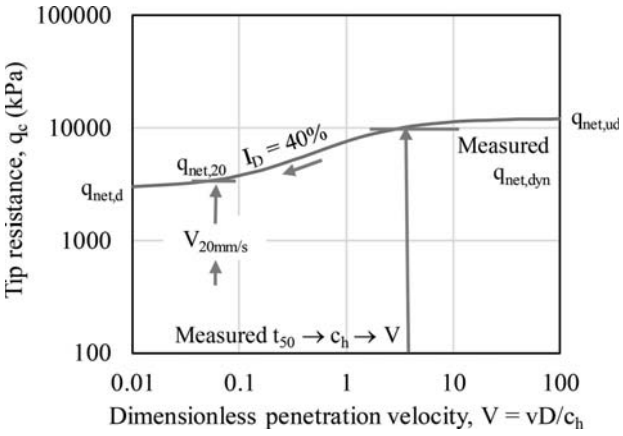

Figure 4. Illustration of interpretation scheme.

only a minor variation in the penetration resistance or the inferred relative density. For this reason, minor refinements in the adopted dissipation solution have only minimal effect on the model.

The log scale hides the significant range in penetration resistance: a change in relative density of 5% typically leads to a change in penetration resistance of ~15% in drained conditions. In undrained conditions, a 5% change in I_D doubles the undrained penetration resistance at low relative density, but has only a 10% effect close to $I_D = 1$.

The practical approach for using this models to interpret FFP results is shown in Figure 4. At all depths within the deceleration response, the measured q_c can be combined with the current V that is inferred using the c_h derived from the final dissipation test. This (q_c,V) pair identifies a relative den-

sity line, which can then be used to determine the drained limit, $q_{c,d}$ (or $q_{c,20}$, the penetration resistance at the standard rate of 20 mm/s) as well as the undrained limit, $q_{c,ud}$.

6 SYNTHETIC FFP ANALYSES

To illustrate the behavior of the model, a set of synthetic FFP penetration responses have been generated for uniform sand, with the parameters given earlier in this paper, and assuming a consolidation coefficient of $c_h = 10^6$ m^2/year. The penetrometer is idealized as a 0.1 m diameter cone with a 60° tip, one metre in length, of solid steel. Shaft resistance is neglected.

Firstly, the responses in uniform loose and medium dense sand are compared for a range of impact velocities from 2.5–10 m/s, which are typical for FFPs (Young et al. 2011, Stark et al 2009). The assumption that relative density is constant with depth is adopted here, but may not apply in real sediments.

In loose sand (Figure 5), the synthetic dynamic resistance, $q_{c,dyn}$, is initially close to the undrained limit, $q_{c,u}$, but as the penetrometer decelerates the resistance converges to the drained limit, $q_{c,d}$.

In this soil, the conventional CPT profile (marked $q_{c,0.02}$) is fully drained. Below the initial few centimetres, the loose sand is contractile, so slowing of the probe is accompanied by an increase in resistance. A conventional rate effect correction that reduces the resistance with strain rate (or velocity) would not be appropriate in a contractile soil since it would adjust the measured resistance downwards instead of upwards. A viscous rate effect could be added into this model, but would have a minor effect relative to drainage.

Having determined these equivalent values of penetration resistance, any interpretation that is conventionally applied to the push-in cone tip resistance can also be applied. Where relative density is required, it is already known directly from the interpretation process.

The medium dense sand (Figure 6) is dilatant, so the opposite trend is evident. The rate effect due to drainage is much stronger than a conventional viscous-type rate effect. A four-fold increase in velocity causes an approximate doubling of resistance.

The effect of relative density is highlighted in Figure 7. The fully drained and fully undrained profiles of tip resistance are shown for a range of relative densities, along with FFP responses for an impact velocity of 10 m/s.

These profiles highlight the stronger effect of density on undrained tip resistance compared to drained tip resistance. This suggests that the penetration resistance in an FFP test could be a more sensitive measure of density variations than a conventional cone (although such detection of density gradations in an FFP test requires the drainage-based interpretation in this paper). Figure 7 also highlights the rapidity of the deceleration in dense sands, emphasizing the need for rapid data logging. For $I_D = 0.75$, the full deceleration takes <0.01 seconds.

A limitation of the analyses presented, which also applies to static CPTs, is that they rely on Equations 3 and 6 for penetration resistance, which

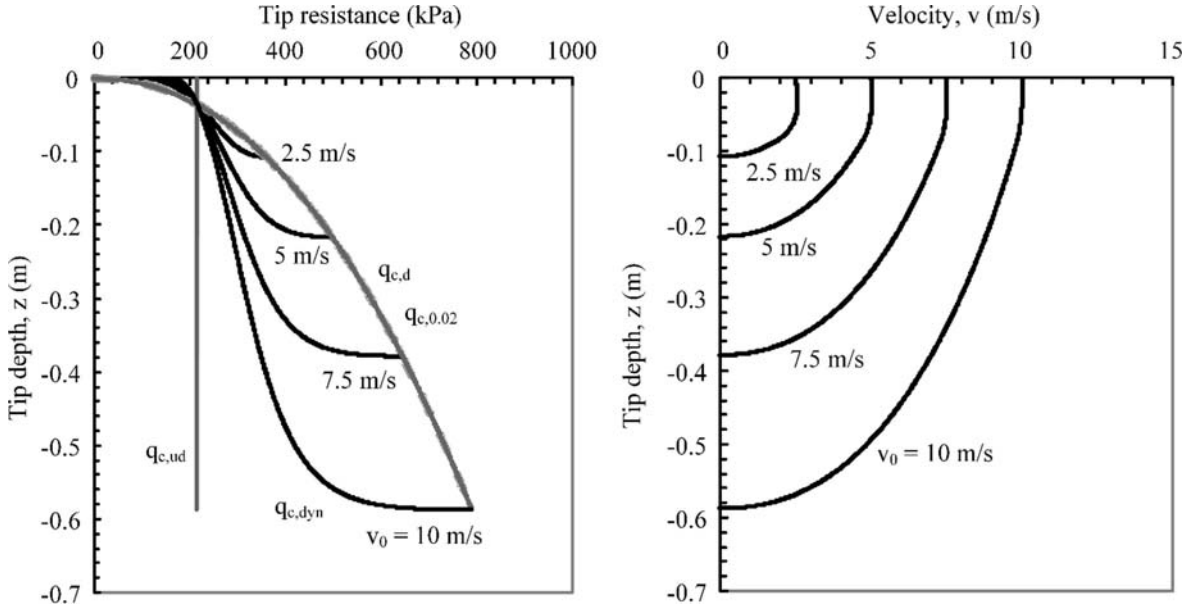

Figure 5. Synthetic responses in loose sand ($I_D = 0.15$) for varying impact velocity.

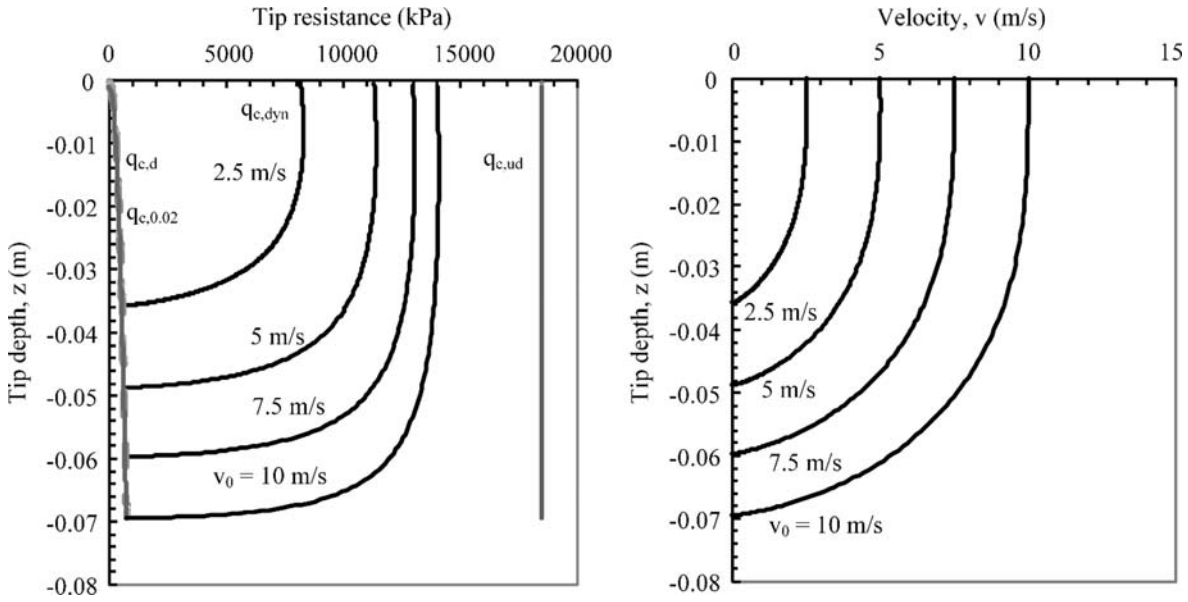

Figure 6. Synthetic responses in medium dense sand ($I_D = 0.45$) for varying impact velocity.

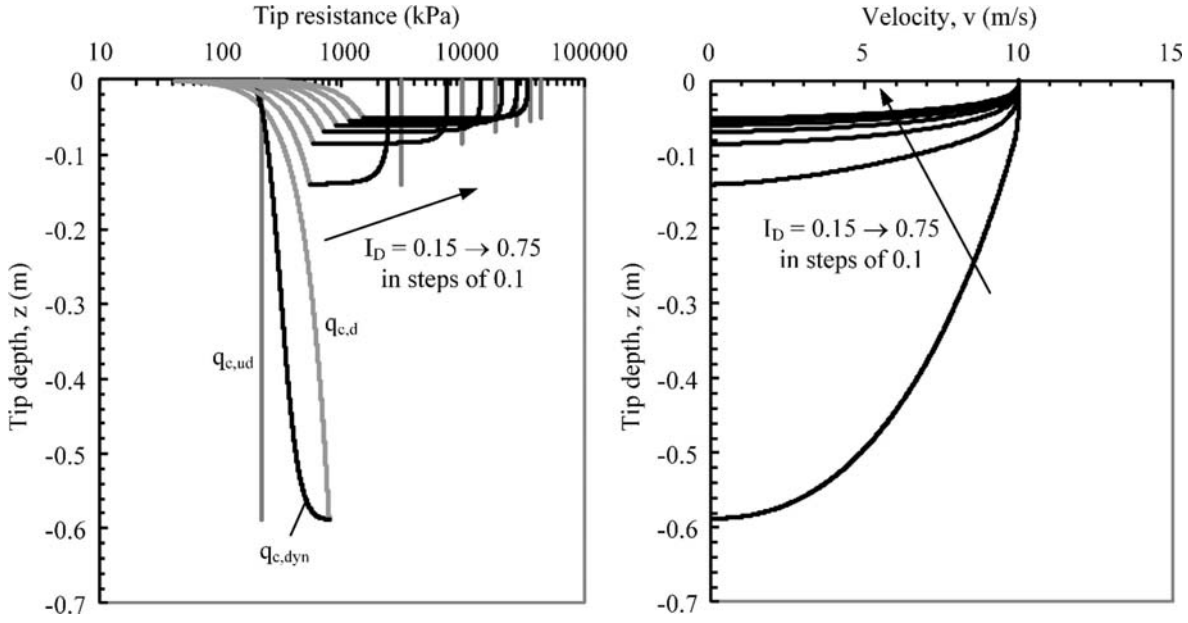

Figure 7. Synthetic responses for varying relative density.

are strictly for deep penetration, whereas lower bearing factors apply at shallow embedment.

7 CONCLUSIONS

A simple new procedure to interpret free fall penetration tests in sandy soils has been outlined. The method extends existing approaches that consider only viscous-type rate effects. The method introduces a simple approach to the effect of drainage on penetration resistance using a model for sand that captures the effect of relative density on both the drained and undrained penetration resistance. This model uses Bolton's correlations to define the undrained strength of sand at a given density, and conventional correlations to link (drained) cone resistance to relative density.

Using this model, the FFP resistance during deceleration in undrained or partially drained conditions can be uniquely mapped to a resistance from a standard CPT, when combined with a consolidation coefficient derived from the dissipation response.

With development and validation, this new framework could enhance the value of FFPs as a complementary or alternative technology alongside conventional static penetration testing.

REFERENCES

Albatal A. & Stark N. 2017. Rapid sediment mapping and in situ geotechnical characterization in challenging aquatic areas. Limnol. Oceanogr.: Methods 15, 2017, 690–705.

Aubeny, C.P. & Shi H. 2006.Interpretation of impact penetration measurements in soft clays: ASCE Journal of Geotechnical and Geoenvironmental Engineering, 132:770–777.

Bolton M.D. 1986. The strength and dilatancy of sands. Geotechnique, 36(1), 65–78.

Chatterjee, S. Gourvenec, S.M & White D.J. 2014. Assessment of the consolidated breakout response of partially embedded seabed pipelines. Géotechnique 64(5): 391–399.

Chow, S.H., O'Loughlin, C.D. & Randolph, M.F. 2014. Soil strength estimation and pore pressure dissipation for free-fall piezocones in soft clay. Geotechnique 64(10):817–827.

Chow S.H., O'Loughlin C.D., White D.J. & Randolph M.F. 2017. An extended interpretation of the free-fall piezocone test in clay. Géotechnique. 67(12):1090–1103.

Colreavy, C, O'Loughlin, C & Randolph, M (2016). Estimating consolidation parameters from field piezoball tests Géotechnique, 66(4): 333–343.

Emerson. M., Foray, P., Puech, A. & Palix, E. 2008. A global model for accurately interpreting CPT data in sands from shallow to greater depth. Int. Conf. Geotechnical and Geophysical Site Characterization. 687–694 Taylor & Francis.

Jamiolkowski, M.B., Lo Presti, D.C.F. & Manassero, M. 2003. Evaluation of relative density and shear strength of sands from cone penetration test (CPT) and flat dilatometer (DMT), Soil Behaviour and Soft Ground Construction, ASCE, GSP 119, 201–238.

Lunne, T., Andersen, K.H., Low, H.E., & Randolph, M.F. 2011. Guidelines for offshore in situ testing and interpretation in deepwater soft clays. Can. Geotech. J. 48,543–556.

Mahmoodzadeh, H., Wang, D. and Randolph, M.F. 2015. Interpretation of piezoball dissipation testing in clay. Géotechnique, 65(10): 831–842.

Mayne, P.W. 2014. Keynote: Interpretation of geotechnical parameters from seismic piezocone tests. Proc. 3rd Int. Symp. Cone Penetration Testing, CPT'14, 47–73.

Mumtaz, M.B., Stark N. & Brizzolara S. 2018. Pore pressure measurements using a portable free fall penetrometer. Proc. CPT '18, Delft (this proceedings).

Mulukutla, G.K. 2009. Determination of geotechnical properties of seafloor sediment. PhD thesis, U. New Hamp., USA.

Randolph, M.F. & Hope, S. 2004. Effect of cone velocity on cone resistance and excess pore pressures. Proc. Int. Symp. Deformation Characteristics of geo- materials, 147–152.

Randolph, M.F. 2004 Characterisation of soft sediments for offshore applications. 2nd International Site Character-ization Conference, Porto, Portugal, Vol. 1, pp. 209–232.

Randolph M.F., Jamiolkowski M.B. & Zdravkovic L. 2004. Load carrying capacity of foundations. Proc. Skempton Memorial Conference. 207–240.

Robertson P.K. 1990. Soil classification using the cone penetration test. Canadian Geotechnical Journal, 27(1): 151–158.

Stark,N., Hanff, H. & Kopf A. 2009. Nimrod: a tool for rapid geotechnical characterization of surface sediments. Sea Technology 50 (4), 10–14.

Steiner, A., Kopf, A.J., L'Heureux, J.-S., Kreiter, S., Stegmann, S., Haflidason, H. & Moerz, T. 2014. In situ dynamic piezocone penetrometer tests in natural clayey soils–a reappraisal of strain-rate corrections. Can. Geotech. J. 51, 272–288.

Sully, J.P., Robertson, P.K., Campanella, R.G. & Woeller, D.J. (1999). An approach to evaluation of field CPTU dissipation data in overconsolidated fine-grained soils. Canadian Geotechnical Journal 36, No. 2, 369–381.

Young, A.G., Bernard, B.B., Remmes, B.D., Babb, L. & Brooks, J.M. (2011). CPT Stinger - an innovative method to obtain CPT data for integrated geoscience studies. Offshore Technology Conf.. Houston, Texas, United States.

View publication stats